



Exact free vibration analysis for membrane assemblies with general classical boundary conditions



Xiang Liu ^{a, b, c, d, *}, Xueyi Zhao ^{a, b, d}, Chen Xie ^{a, b, d, **}

^a Key Laboratory of Traffic Safety on Track (Central South University), Ministry of Education, Central South University, Hunan, Changsha, 410075, China

^b Joint International Research Laboratory of Key Technology for Rail Traffic Safety, Central South University, Hunan, Changsha, 410075, China

^c State Key Laboratory of High Performance Complex Manufacturing, Central South University, Hunan, Changsha, 410075, China

^d School of Traffic & Transportation Engineering, Central South University, Hunan, Changsha, 410075, China

ARTICLE INFO

Article history:

Received 17 January 2020

Received in revised form 22 May 2020

Accepted 25 May 2020

Available online 4 July 2020

Handling Editor: S. Ilanko

Keywords:

Dynamic stiffness method

Modal analysis

Membranes

General classical boundary conditions

Wittrick-Williams algorithm

ABSTRACT

This paper proposes exact dynamic stiffness formulations for membranes and their assemblies under any arbitrary classical boundary conditions. First, by taking exact solutions in one direction satisfying all possible opposite edge supports, we can derive exact general solutions of the Helmholtz equation for membrane vibration. Then, generic force and displacement boundary conditions in the other direction are expressed in terms of the general solutions. Finally, the dynamic stiffness matrices of rectangular membrane elements are formulated, which can be assembled directly and allows applications of arbitrary boundary conditions. As an accurate and efficient modal solution technique, the Wittrick-Williams (WW) algorithm is applied onto the global dynamic stiffness matrix of the final structure. The most important issue of the WW algorithm, J_0 count, has been resolved with the analytical expressions derived for all possible cases. The proposed dynamic stiffness method (DSM) is then applied to several examples including individual membranes and their assemblies. High accuracy and exactness of the proposed method within the whole frequency range is demonstrated by comparison with the finite element method. Besides, interesting findings have been observed on repeated eigenvalues with distinct mode shapes corresponding to certain aspect ratio and tension ratio, where physical and mathematical understanding has been provided.

© 2020 Elsevier Ltd. All rights reserved.

1. Introduction

Membrane structures have been widely used in nature and engineering. For example, due to the outstanding foldable, inflatable and light-weighted merits, membranes are been increasingly used in space structures for antennae, reflectors and solar arrays [1,2]. Since membrane's vibrations are very sensitive to acoustic excitations, they have been an ideal receiver and measuring tool such as eardrums, sound transducers and sound field visualizers. Also, the vibrating properties of membranes

* Corresponding author. Key Laboratory of Traffic Safety on Track (Central South University), Ministry of Education, Central South University, Hunan, Changsha, 410075, China.

** Corresponding author. Joint International Research Laboratory of Key Technology for Rail Traffic Safety, Central South University, Hunan, Changsha, 410075, China.

E-mail addresses: xiangliu06@gmail.com (X. Liu), zxy563675400@csu.edu.cn (X. Zhao), 174212084@csu.edu.cn (C. Xie).

are made use of in generating sound in musical instruments, louder speakers, and for filtration purposes in ultrafiltration membranes, etc. [3,4]. Therefore, investigations on the vibration characteristics of membrane structures relating to the above important functionalities have been an inevitable topic in a diverse array of application fields.

There have been many attempts to investigate the vibration of membranes by many researchers in past decades. They cover homogenous and non-homogenous models, simple and arbitrary shaped geometric configurations. Nevertheless, existing exact solutions are only applicable to homogeneous membranes with a simple geometry such as a rectangle or circle [5–9] and with certain boundary conditions. For membranes and their assemblies with non-homogeneous material and tensile stresses or complex boundary conditions, however, we need to resort to approximate numerical or semi-analytical solutions, including the collocation approach [10–12], Rayleigh-Ritz method [13,14], finite difference method [15], direct, indirect and multipole Trefftz method [16–18], discrete singular convolution method [19–21], non-dimensional dynamic influence function method [22–24], differential quadrature method [25], wave propagation method [26,27], boundary element method [28–30], finite element method (FEM) [31–38], and spectral element method (SEM) [39,40], null-field integral method for a specific group of membranes [41–44].

Among various different methods, the FEM is one of the most universally employed typical numerical method for complex engineering structures. Nevertheless, more elements are required to achieve results with higher accuracy due to the adopted approximate shape functions, which will increase the computational dramatically, particularly in higher frequency ranges. Thus, the FEM is not suitable for analysis within mid to high frequency ranges.

In contrast to the FEM, there is an analytical method for vibration analysis known as the dynamic stiffness method (DSM). In DSM, the shape functions are essentially the exact general solutions derived from the frequency-dependent governing differential equations. Accordingly, exact modal analysis of the structures can be carried out within the whole frequency range by using only one or few elements with very few degrees of freedom. Furthermore, an efficient and robust algorithm proposed by Wittrick and Williams [45] is applied to compute natural frequencies with any required precision and it guarantees that no natural frequency is missed. This is in a sharp contrast to existing analytical methods [6,26,40] and commercial finite element software. In addition, another advantage over other analytical methods is that each individual element in the DSM can be assembled directly, which is similar to the FEM. Therefore, structures with assembly, boundary conditions and inhomogeneity can be modelled. Many researchers have devoted considerable efforts to dynamic stiffness (DS) theories in the past. For example, Banerjee et al. [46–48] developed one-dimensional DS elements for a wide range of bars and beams and produced a well-developed software called BUNVIS-RG [49]. For two-dimensional structures like plates, the DS formulation for plate assemblies with Levy-type boundary conditions was developed by Wittrick and Williams [50] for the first time, and then researchers developed the DS plate theory for the vibrations of Kirchhoff plates [51–53], Mindlin plates [54], and composite plates [55–58] as well as buckling problems [59,60]. Despite of the importance of membrane vibration and the advantages of the DSM, there have been no literature on the development of the DS matrix of membranes and their assemblies subjected to arbitrary boundary conditions.

To fill this gap, the main aim of this paper is to propose dynamic stiffness (DS) formulations for rectangular membranes and their assemblies subjected to any arbitrary boundary conditions. First, the exact general solution of differential equations governing membrane vibration is obtained in the frequency domain by the method of separation of variables. Then, the force and displacement relationship in the frequency domain is established in the form of DS matrix by applying the corresponding boundary conditions whilst eliminating the constant vector in the general solution. For membrane assemblies, the elemental DS matrices of all membrane elements are assembled directly to form the global DS matrix of the overall structure. Any arbitrary boundary conditions can be applied directly to the global DS matrix. Then, the Wittrick-Williams (WW) algorithm is applied onto the global DS matrix to compute the natural frequencies. One of the essential issues in the WW algorithm that the natural frequencies of membrane elements clamped on all nodal edges is resolved analytically in this research. The

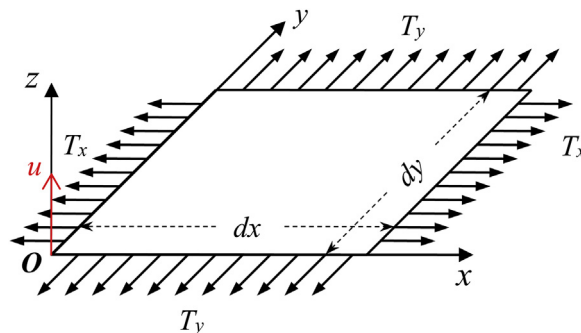


Fig. 1. Displacements and forces of a rectangular membrane element.

exactness and high computational efficiency of the proposed DSM is validated by comparison with the conventional FEM in several computational exercises.

This paper is organized as follows. Section 2 is devoted to the development of dynamic stiffness formulations and implementation of the Wittrick-Williams (WW) algorithm. The governing differential equation and boundary conditions for free vibration of a membrane are provided in Section 2.1. Then dynamic stiffness formulations for a rectangular membrane element under different combinations of principal boundary conditions (PBCs) are derived in Section 2.2. Next, Section 2.3 describes the assembly procedure and the application of nodal boundary conditions. In Section 2.4, the WW algorithm is applied with all J_0 counts under different PBCs developed. Section 3 is the result section. Section 3.1 shows the application of present theory to individual membranes and demonstrates the high efficiency and exactness; some interesting findings on the mode shapes are also given. Section 3.2 applies the DSM to the modal analysis of a membrane assembly. Finally, conclusions are drawn in Section 4.

2. Theory

2.1. Governing differential equation and boundary conditions for free vibration of a membrane

2.1.1. Governing differential equation

Consider a homogeneous and flexible membrane shown in Fig. 1. The membrane is assumed to vibrate transversely, and the deflection $u(x, y, t)$ is assumed to be very small compared with the size of the membrane. Therefore, the linear free vibration of membrane is studied based on the theory of small deflection. By using the Hamilton's principle, the governing differential equation (GDE) for the transverse vibration of the membrane can be derived as follows.

$$T_x \frac{\partial^2 u}{\partial x^2} + T_y \frac{\partial^2 u}{\partial y^2} - \rho \frac{\partial^2 u}{\partial t^2} = 0 \quad (1)$$

where T_x is the tension per unit length in the x direction whereas T_y is that in the y direction. $u = u(x, y, t)$ is the deflection of the membrane. ρ is the mass per unit area.

The equation governing membrane deflection can be assumed to be $u(x, y, t) = U(x, y)e^{i\omega t}$ due to the free vibration, if the following notations are introduced

$$\beta = \frac{T_y}{T_x}, \quad k = \frac{\omega}{c}, \quad c = \sqrt{\frac{T_x}{\rho}} \quad (2)$$

then Eq. (1) can be transformed into the frequency domain as follows.

$$\frac{\partial^2 U}{\partial x^2} + \beta \frac{\partial^2 U}{\partial y^2} + k^2 U = 0. \quad (3)$$

Particularly, $\beta = 1$ when the membrane is subjected to equivalent bidirectional tensile forces.

2.1.2. Boundary conditions

Fig. 2 shows displacement and force boundary conditions (BCs) on four edges of a rectangular membrane, where b and l is the length and width, respectively. Boundaries \mathcal{L}_2 and \mathcal{L}_4 serve as principal boundaries (PBs) whereas boundaries \mathcal{L}_1 and \mathcal{L}_3 are denoted by nodal boundaries (NBs) which can be used for membrane assemblies. The displacement and force BCs on four membrane edges can be expressed as

$$\mathcal{L}_1 : \begin{cases} U_1(y) = U(x=b, y) \\ P_1(y) = T_x \frac{\partial U}{\partial x}(x=b, y) \end{cases}, \quad \mathcal{L}_3 : \begin{cases} U_3(y) = U(x=0, y) \\ P_3(y) = -T_x \frac{\partial U}{\partial x}(x=0, y) \end{cases}, \quad (4)$$

$$\mathcal{L}_2 : \begin{cases} U_2(x) = U(x, y=l) \\ P_2(x) = T_y \frac{\partial U}{\partial y}(x, y=l) \end{cases}, \quad \mathcal{L}_4 : \begin{cases} U_4(x) = U(x, y=0) \\ P_4(x) = -T_y \frac{\partial U}{\partial y}(x, y=0) \end{cases}, \quad (5)$$

where P_i and U_i were introduced respectively for the force and displacement BCs prescribed along the boundary \mathcal{L}_i ($i = 1, 2, 3, 4$, see Fig. 2). More specifically, P_2, U_2 and P_4, U_4 are the principal boundary conditions (PBCs) along the boundary \mathcal{L}_2 and \mathcal{L}_4 while P_1, U_1 and P_3, U_3 are the nodal boundary conditions (NBCs) along the boundary \mathcal{L}_1 and \mathcal{L}_3 .

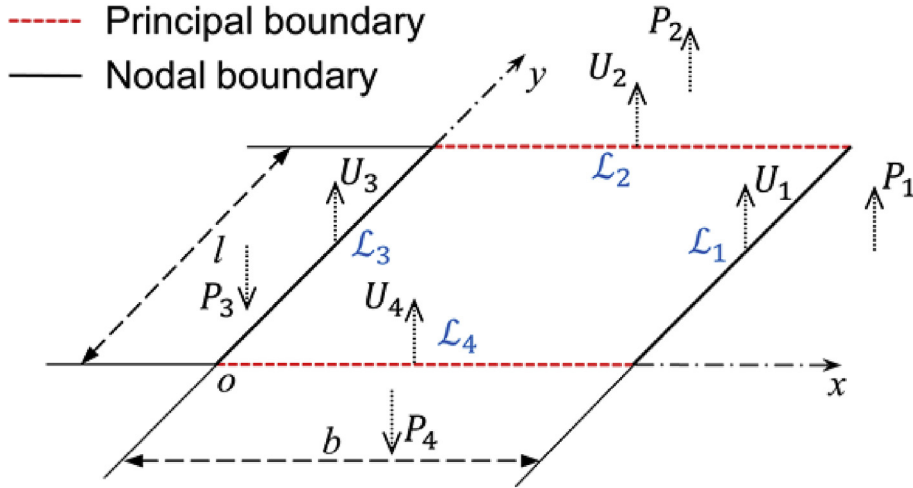


Fig. 2. Boundary conditions applied on four edges of a rectangular membrane.

For each edge of the membrane, two boundary constraints, namely fixed or free, can be prescribed. The fixed or clamped edge is denoted by the letter 'C' and the free edge is represented by the letter 'F'. For a clamped edge, $U_i = 0$ ($i = 1, 2, 3, 4$). For a free edge, $P_i = 0$ ($i = 1, 2, 3, 4$). For a membrane element, there are three combinations for the PBCs: C-C, C-F(F-C), F-F as shown in Fig. 3, where C-F and F-C are equivalent (Note that a single membrane element also has three combinations for the NBCs: C-C, C-F(F-C), F-F. Hence, there are in total nine combinations of BCs for a rectangular membrane: CCCC, FCFC, FCCC, FFFF, CFCF, FFCC, CCCC, FCFF, FCCF). Next, the dynamic stiffness formulations of the rectangular membrane element under all possible PBCs will be deduced and any arbitrary classical BCs can be prescribed along the NBs, therefore the formulation developed in this paper can be applicable to the rectangular membrane under any arbitrary classical boundary conditions.

2.2. Dynamic stiffness formulation for a rectangular membrane element

Dynamic stiffness formulations will be derived based on the GDE of Eq. (3) (see Section 2.1.1) for three different combinations of principal boundary conditions (PBCs) (see Section 2.1.2). Firstly, the exact shape functions of membrane vibration with unknowns are obtained by solving the GDE of Eq. (3) under three different PBCs. Then, the unknown coefficients are eliminated from the expressions of the displacement and force nodal boundary conditions (NBCs) in terms of the general solutions. Subsequently, explicit expressions of the dynamic stiffness matrix for the membrane element under three different PBCs can be obtained. Finally, the membrane elements can be assembled at shared nodal boundaries (NBs) and any arbitrary BCs can be applied on the NBs (see Section 2.3.1).

In order to satisfy the three different PBCs as shown in Fig. 3, the general solutions of Eq. (3) should take the forms as follows.

$$U(x, y) = \begin{cases} \sum_{m=1}^{\infty} X_m(x) \sin(\alpha_m y), & \text{C - C or C - F} \\ \sum_{m=0}^{\infty} X_m(x) \cos(\alpha_m y), & \text{F - F} \end{cases} \quad (6)$$

with

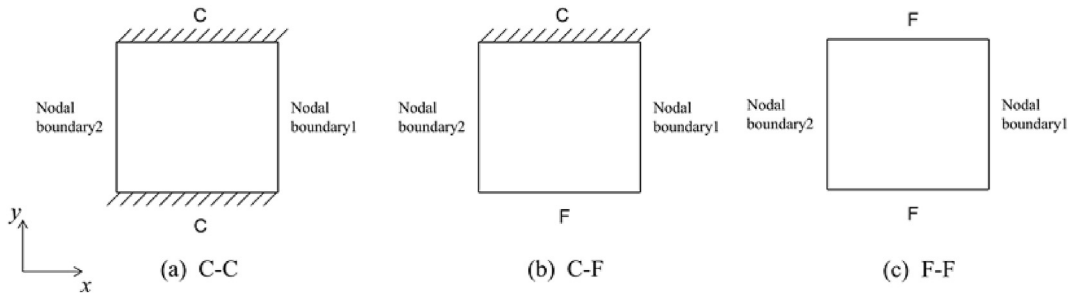


Fig. 3. Three combinations of principal boundary conditions (PBCs) for a rectangular membrane element.

$$\alpha_m = \begin{cases} \frac{m\pi}{l}, m = 1, 2, 3, \dots, & \text{C - C} \\ \frac{m\pi}{l}, m = 0, 1, 2, \dots, & \text{F - F} \\ \left(m - \frac{1}{2}\right)\pi, m = 1, 2, 3, \dots, & \text{C - F} \end{cases} \quad (7)$$

where m denotes the half wave number of a rectangular membrane element in the y direction.

Substituting Eq. (6) into Eq. (3) gives

$$\frac{d^2 X_m}{dx^2} - \lambda^2 X_m = 0 \quad (8)$$

where

$$\lambda = \sqrt{\beta \alpha_m^2 - k^2} \quad (9)$$

The general solution of Eq. (8) can be written as

$$X_m(x) = C_1 \cosh \lambda x + C_2 \sinh \lambda x \quad (10)$$

where C_1 and C_2 are constants.

The transverse component of the tension in the x direction of the membrane $P_m(x, y)$ can be expressed as

$$P_m(x, y) = T_x \frac{\partial U}{\partial x} = \begin{cases} P_m(x) \sin(\alpha_m y) & \text{C - C or C - F} \\ P_m(x) \cos(\alpha_m y) & \text{F - F} \end{cases} \quad (11)$$

where

$$P_m(x) = T_x \frac{dX_m}{dx} = T_x \lambda (C_1 \sinh \lambda x + C_2 \cosh \lambda x) \quad (12)$$

Referring to Fig. 2, the displacement and force BCs on the nodal boundaries (NBs) can be recast as follows.

$$\text{At } x=0, X = U_3, P = -P_3 \quad (13)$$

$$\text{At } x=b, X = U_1, P = P_1 \quad (14)$$

Substituting Eqs. (13) and (14) into Eqs. (10) and (12), the relationships between displacement vector and constant vector, force vector and constant vector can be derived respectively.

$$\mathbf{d} = \begin{Bmatrix} U_1 \\ U_3 \end{Bmatrix} = \begin{bmatrix} \cosh \gamma & \sinh \gamma \\ 1 & 0 \end{bmatrix} \begin{Bmatrix} C_1 \\ C_2 \end{Bmatrix} \quad (15)$$

$$\mathbf{f} = \begin{Bmatrix} P_1 \\ P_3 \end{Bmatrix} = T_x \lambda \begin{bmatrix} \sinh \gamma & \cosh \gamma \\ 0 & -1 \end{bmatrix} \begin{Bmatrix} C_1 \\ C_2 \end{Bmatrix} \quad (16)$$

where

$$\gamma = \lambda b \quad (17)$$

The constants C_1 and C_2 can now be eliminated from Eqs. (15) and (16) to give the relationship between force vector \mathbf{f}^e and displacement vector \mathbf{d}^e , so the dynamic stiffness matrix can be derived taking the following form

$$\begin{Bmatrix} P_1 \\ P_3 \end{Bmatrix} = \begin{bmatrix} a_1 & a_2 \\ a_2 & a_1 \end{bmatrix} \begin{Bmatrix} U_1 \\ U_3 \end{Bmatrix} \quad (18)$$

or

$$\mathbf{f}^e = \mathbf{K}^e(\omega) \mathbf{d}^e \quad (19)$$

where $\mathbf{K}^e(\omega)$ is the dynamic stiffness matrix of a rectangular membrane element with

$$a_1 = \frac{T_x}{b} \gamma \coth \gamma, \quad a_2 = -\frac{T_x}{b} \gamma \operatorname{csch} \gamma \quad (20)$$

The derivation of Eqs. (8)–(20) above is applicable to the membrane elements under all three kinds of PBCs in Eq. (7).

2.3. Assembly procedure and the application of nodal boundary conditions

After obtaining the dynamic stiffness matrix of the membrane element $\mathbf{K}^e(\omega)$, the global dynamic stiffness matrix $\mathbf{K}^g(\omega)$ can be obtained by assembling the membrane elements as illustrated in what follows.

Fig. 4 presents an example illustrating the assembly procedure of membrane elements. Suppose that there are three membrane elements (E1 E2 and E3) to be assembled, and the dynamic stiffness matrices of each membrane element are \mathbf{K}^{E1} , \mathbf{K}^{E2} and \mathbf{K}^{E3} . Membrane elements E1 and E2 share nodal boundary 1(7) while membrane elements E2 and E3 share nodal boundary 5(11). If \mathbf{f}^g and \mathbf{d}^g are the force and displacement vectors of the four nodal boundaries 3, 1(7), 5(11) and 9 of the membrane assembly respectively, then the dynamic stiffness matrix of a membrane assembly takes the following form

$$\mathbf{f}^g = \mathbf{K}^g(\omega) \mathbf{d}^g \quad (21)$$

where

$$\mathbf{f}^g = \{f_1 \ f_2 \ f_3 \ f_4\}^T, \quad \mathbf{d}^g = \{d_1 \ d_2 \ d_3 \ d_4\}^T, \quad (22)$$

$$\mathbf{K}^g(\omega) = \begin{bmatrix} k_{11}^{E1} & k_{12}^{E1} & 0 & 0 \\ k_{21}^{E1} & k_{22}^{E1} + k_{11}^{E2} & k_{12}^{E2} & 0 \\ 0 & k_{21}^{E2} & k_{22}^{E2} + k_{11}^{E3} & k_{12}^{E3} \\ 0 & 0 & k_{21}^{E3} & k_{22}^{E3} \end{bmatrix}$$

Once the assembly procedure is accomplished, any arbitrary classical BCs can be applied to the nodal boundaries of the membrane assembly (3, 9 as shown in Fig. 4). If all four edges 3, 1, 5, 9 are free, which leads to $\mathbf{K}^g \mathbf{d}^g = 0$. If any degree of freedom (DOF) is constrained, the rows and columns of the global dynamic stiffness matrix corresponding to the DOF whose displacement is zero are removed. For example, if 3 and 9 are fixed edges while 1 and 5 are free edges, then the displacement vector with prescribed constraints becomes $\mathbf{d}^f = \{d_2 \ d_3\}^T$ and the global dynamic stiffness matrix for the final structure with prescribed boundary conditions $\mathbf{K}^f(\omega)$ can be written as

$$\mathbf{K}^f(\omega) = \begin{bmatrix} k_{22}^{E1} + k_{11}^{E2} & k_{12}^{E2} \\ k_{21}^{E2} & k_{22}^{E2} + k_{11}^{E3} \end{bmatrix} \quad (23)$$

Next, natural frequencies and mode shapes of either an individual membrane or membrane assemblies can be computed from the global dynamic stiffness matrix for the final structure by using eigenvalue solution techniques as described next.

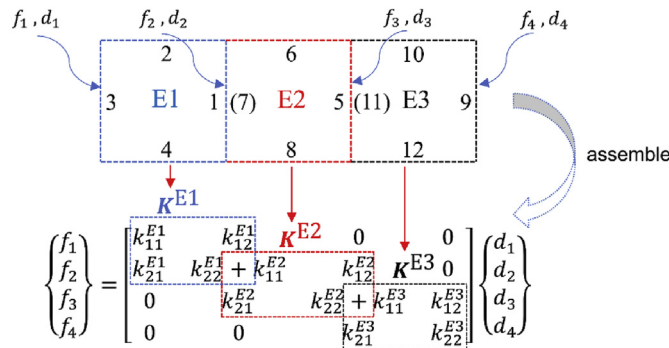


Fig. 4. Assembly procedure of membrane elements.

2.4. Wittrick-Williams modal algorithm

Wittrick-Williams (WW) algorithm is a precise and efficient solution technique for free vibration analysis based on dynamic stiffness formulations. This algorithm also guarantees that no natural frequencies and mode shapes will be missed. Suppose that ω denotes the circular frequency of membrane vibration and ω^* represents a given trial frequency ($\omega^* \geq 0$), then according to the WW algorithm, the number of natural frequencies below the trial frequency J is given by

$$J = J_0(\omega^*) + s\{\mathbf{K}(\omega^*)\} \quad (24)$$

where $s\{\mathbf{K}(\omega^*)\}$ is the number of negative elements on the leading diagonal of $\mathbf{K}^A(\omega^*)$, which is the upper triangular matrix transformed by the Gauss elimination of $\mathbf{K}(\omega)$ at $\omega = \omega^*$, and $J_0(\omega^*)$ can be derived by

$$J_0(\omega^*) = \sum_e J_{0m}^e(\omega^*) \quad (25)$$

where $J_{0m}^e(\omega^*)$ is the number of natural frequencies below the trial frequency for each individual membrane element when its nodal boundaries are clamped under a chosen value of m . It is easily seen that, $s\{\mathbf{K}(\omega^*)\}$ is determined by the nodal boundary conditions (NBCs) of the membrane elements (All the principal boundary conditions (PBCs) have been determined) and J_0 depends on PBCs (All the nodal boundaries (NBs) of the membrane elements are fixed).

It can be seen from Eq. (24) that J_0 count is a crucial step in the application of WW algorithm. In the following, the derivation of the expression of J_0 with different PBCs and fixed NBs is introduced in detail. Firstly, according to the BCs of the membrane, the expressions between the natural frequency ω_{nm} and m, n are obtained under different PBCs, m and n stand for the half wave number in the x and y directions respectively. Then, the solution of n is derived by solving the expression of ω_{nm} with respect to m and n at a certain trial frequency. Consequently, $J_{0m}^e(\omega^*)$ is obtained by the definition given in Eq. (25) and further J_0 problem can be derived.

(1) C-C PBC

When the BCs of the membrane element is CCCC, the eigenfunction or mode shape $U_{nm}(x, y)$ corresponding to the natural frequency ω_{nm} is given by

$$U_{nm}(x, y) = C_{nm} \sin \frac{n\pi x}{b} \sin(\alpha_m y), \quad m, n = 1, 2, \dots \quad (26)$$

The general solution of Eq. (3) takes the following form

$$U(x, y) = \sum_{n=1}^{\infty} \sum_{m=1}^{\infty} C_{nm} \sin \frac{n\pi x}{b} \sin(\alpha_m y) \quad (27)$$

Substituting Eq. (27) into Eq. (3) gives the relationship between ω_{nm} and m, n under C-C PBC.

$$\omega_{nm}^{cc} = \pi c \sqrt{\left(\frac{n}{b}\right)^2 + \beta \left(\frac{m}{l}\right)^2}, \quad m, n = 1, 2, \dots \quad \text{CCCC} \quad (28)$$

(2) F-F PBC

When the BCs of the membrane element is CFCF, mode shape $U_{nm}(x, y)$ can be expressed as

$$U_{nm}(x, y) = C_{nm} \sin \frac{n\pi x}{b} \cos(\alpha_m y), \quad m = 0, 1, \dots, n = 1, 2, \dots \quad (29)$$

The general solution of Eq. (3) takes the following form

$$U(x, y) = \sum_{n=1}^{\infty} \sum_{m=0}^{\infty} C_{nm} \sin \frac{n\pi x}{b} \cos(\alpha_m y) \quad (30)$$

Substituting Eq. (30) into Eq. (3), the relationship between ω_{nm} and m, n under F-F PBC is given by

$$\omega_{nm}^{\text{FF}} = \pi c \sqrt{\left(\frac{n}{b}\right)^2 + \beta \left(\frac{m}{l}\right)^2}, \quad m = 0, 1, \dots, n = 1, 2, \dots \quad \text{CFCF} \quad (31)$$

(3) C-F PBC

When the BC of the membrane element is CCCF, mode shape $U_{nm}(x, y)$ becomes

$$U_{nm}(x, y) = C_{nm} \sin \frac{n\pi x}{b} \cos(\alpha_m y), \quad m, n = 1, 2, \dots \quad (32)$$

The general solution of Eq. (3) takes the following form

$$U(x, y) = \sum_{n=1}^{\infty} \sum_{m=1}^{\infty} C_{nm} \sin \frac{n\pi x}{b} \cos(\alpha_m y) \quad (33)$$

Substituting Eq. (33) into Eq. (3), the relationship between ω_{nm} and m, n under C-F PBC can be written as

$$\omega_{nm}^{\text{CF}} = \pi c \sqrt{\left(\frac{n}{b}\right)^2 + \beta \left(\frac{m - \frac{1}{2}}{l}\right)^2}, \quad m, n = 1, 2, \dots \quad \text{CCCF} \quad (34)$$

After obtaining the expressions between ω_{nm} and m, n under different PBCs and fixed nodal boundaries, $J_{0m}^e(\omega^*)$ can now be deduced. According to the definition of $J_{0m}^e(\omega^*)$ in Eq. (25), $J_{0m}^e(\omega^*)$ is actually the number of triangles in the red shaded part of the region covered by the curve l_1 or l_2 (see Fig. 5), therefore, the expressions of $J_{0m}^e(\omega^*)$ under different PBCs can be obtained by solving Eqs. (28), (31) and (34) to get the n at a certain trial frequency respectively.

$$J_{0m}^e(\omega^*) = \left\lfloor \text{Re} \left[\frac{b}{\pi} \sqrt{\left(\frac{\omega^*}{c}\right)^2 - \beta \alpha_m^2} \right] \right\rfloor \quad (35)$$

where $\text{Re}[x]$ means the real part of x and $\lfloor x \rfloor$ is the floor function indicating the largest integer not greater than x .

3. Results

The theory in Section 2 is implemented into an efficient Matlab program, for the exact modal analysis of individual membranes and membrane assemblies. In this section, unless otherwise stated, mass per unit area $\rho = 7.805 \text{ kg/m}^2$, the magnitudes of tension per unit length in both x and y directions are equal to $T = 13800 \text{ N/m}$, and the boundary conditions (BCs) are listed in the anticlockwise sense of $\mathcal{L}_1 - \mathcal{L}_2 - \mathcal{L}_3 - \mathcal{L}_4$ as described in Section 2.1.2. Section 3.1 applies the dynamic stiffness method (DSM, see Section 2.2) to the modal analysis of individual membranes. Section 3.2 illustrates the application of DSM to a membrane assembly.

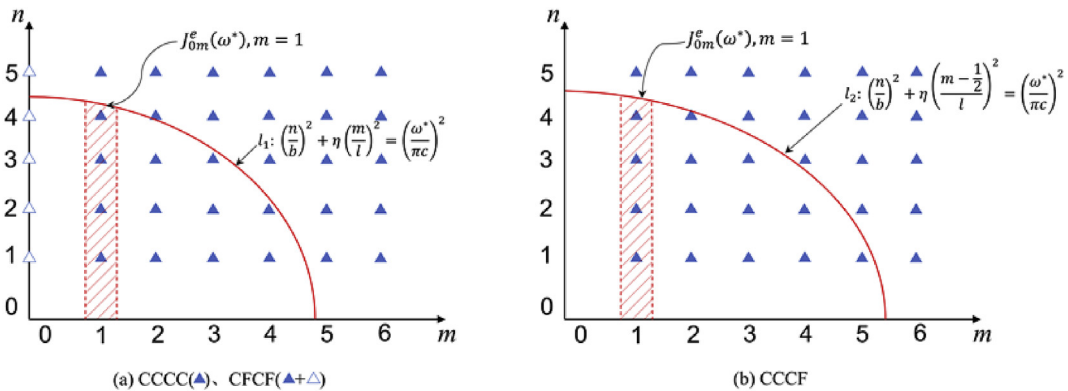


Fig. 5. $J_{0m}^e(\omega^*)$ under three different principal boundary conditions (PBCs).

3.1. Individual membranes

In this section, exact free vibration analysis of individual membranes by using the dynamic stiffness method (DSM) is discussed. Section 3.1.1 demonstrates the high efficiency and accuracy of the DSM. Section 3.1.2 focuses on the effects of aspect ratio η and tension ratio β on the results. Section 3.1.3 explores some interesting characteristics of free vibration mode shapes together with mathematical and physical interpretations.

3.1.1. Accuracy, efficiency and general applicability of boundary conditions (BCs)

In order to demonstrate the efficiency and accuracy of dynamic stiffness method (DSM), comparisons are made for individual membranes by using the DSM and the finite element method (FEM) in three different mesh sizes (100×100 , 200×200 and 400×400). Table 1 exhibits the first 5 and the 50th, 100th and 200th natural frequencies of free vibration for a square membrane ($l = b = 1$ m) under FCFC and FFFF BCs computed by the DSM and commercial software ANSYS. Each particular natural frequency, the eigenvalue ω_{nm} , corresponds to a combination of half wave numbers n and m values as shown in Table 1. It can be seen from Table 1 that the difference between the first three natural frequencies computed by the DSM and FEM is very small (within 0.02%). The discrepancy become enlarged for higher modes. As the mesh become finer, the FEM results gradually converge to the exact results computed by the DSM. For example, when the FE mesh size is 400×400 , the difference between the 200th natural frequency computed by two methods is within 0.1%; however, the FEM takes as long as 410 s to compute the first 200 modes of a square membrane under FCFC BCs while the DSM only costs 0.3 s. It is apparent that the DSM gives exact results covering low to high frequency ranges with much higher efficiency than the FEM. Fig. 6 shows the 1st, 4th and 5th mode shapes of free vibration for a FCFC square membrane computed by the DSM, which match well with those from ANSYS.

Besides, the DSM mentioned in this paper is applicable to the accurate modal analysis of an individual rectangular membrane under all possible combinations of BCs. In Table 2, the first 8 natural frequencies are computed for an individual rectangular membrane ($l = 1$ m, $b = 2$ m) under all nine possible combinations of BCs. Note that the first frequency is zero under FFFF BCs and the corresponding mode is the rigid body mode, this is due to the reason that the Wittrick-Williams algorithm has been applied to ensure that no natural mode is missed.

3.1.2. Effects of aspect ratio and tension ratio on natural frequencies of rectangular membrane

To investigate the dependence of aspect ratio η on the modal properties, the first 8 natural frequencies of an individual equally stretched rectangular membrane under three typical boundary conditions (BCs) with $\eta = l/b = 0.1, 0.5, 1, 2, 4$ are computed in Table 3. As can be seen from Table 3, when the length of one side is fixed and the other side is increased, the natural frequency ω_{nm} will always decrease. As for mode shapes, the half sine wave number will increase first along the longer direction. For example, when $l/b = 0.1$, the half sine wave number in the x direction increases first while that in the y direction remains unchanged.

To study the influence of tension ratio β on the free vibration behaviours, the first 8 natural frequencies of an individual unequally stretched rectangular membrane ($T_x = 13800$ N/m, $\beta = T_y/T_x = 0.1, 0.5, 2, 10, l = 1, b = 2$) under three typical BCs

Table 1

The first 5 and the 50th, 100th and 200th natural frequencies ω (Hz) of free vibration for a square membrane ($1\text{ m} \times 1\text{ m}$) under FCFC and FFFF BCs by using the DSM and FEM. The results of FEM are obtained by using the SHELL41 element in ANSYS with three different mesh sizes (100×100 , 200×200 and 400×400).

Method		Time (s)	Mode							
			1	2	3	4	5	50	100	200
DSM FEM (R.E. %)	FCFC		(0,1)	(1,1)	(0,2)	(2,1)	(1,2)	(1,8)	(5,10)	(15,6)
	100 × 100	0.3	21.024	29.733	42.049	47.012	47.012	169.50	235.06	339.66
		9	21.023	29.731	42.050	46.970	47.056	169.71	236.36	341.25
	200 × 200	50	(-0.01)	(-0.01)	(0.00)	(-0.09)	(0.09)	(0.12)	(0.55)	(0.47)
			21.025	29.734	42.051	46.992	47.037	169.51	235.45	340.36
	400 × 400	410	(0.00)	(0.00)	(0.01)	(-0.04)	(0.05)	(0.00)	(0.16)	(0.21)
			21.023	29.731	42.047	46.998	47.021	169.47	235.17	339.81
	FFFF		(-0.01)	(-0.01)	(0.00)	(-0.03)	(0.02)	(-0.02)	(0.05)	(0.04)
			(0,0)	(0,1)	(1,0)	(1,1)	(0,2)	(4,6)	(8,7)	(3,15)
	DSM FEM (R.E. %)	100 × 100	0.3	0	21.024	21.024	29.733	42.049	151.61	233.49
9			0	21.020	21.030	29.772	41.999	152.01	224.08	323.15
200 × 200		54	(0)	(-0.02)	(0.02)	(0.13)	(-0.12)	(0.27)	(0.26)	(0.48)
			0	21.023	21.027	29.754	42.023	151.78	223.67	322.47
400 × 400		380	(0)	(-0.01)	(0.01)	(0.07)	(-0.06)	(0.12)	(0.08)	(0.27)
			0	21.022	21.024	29.741	42.033	151.68	223.53	321.84
			(0)	(-0.01)	(0.00)	(0.03)	(-0.04)	(0.05)	(0.02)	(0.07)

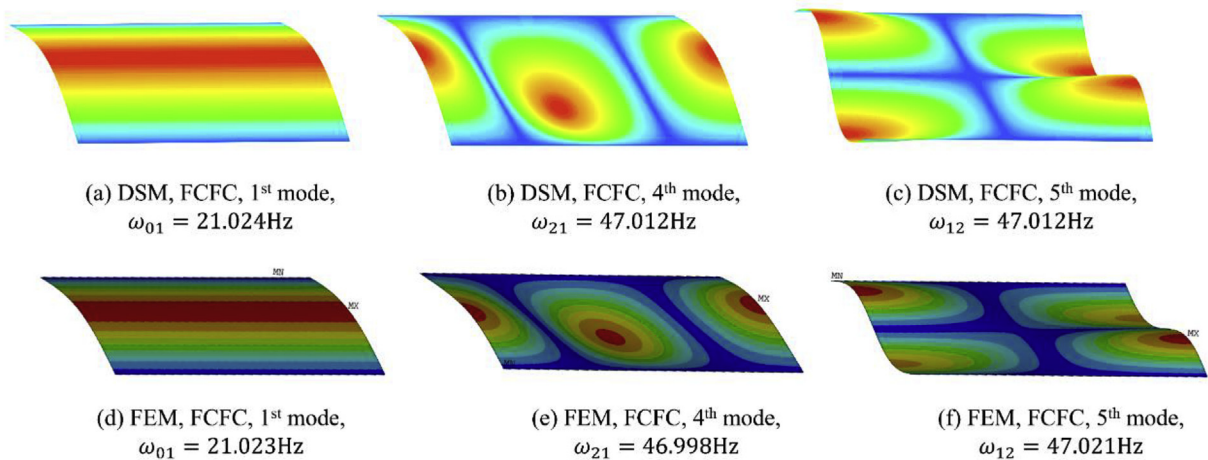


Fig. 6. The 1st, 4th and 5th natural modes of an individual square membrane ($1 \text{ m} \times 1 \text{ m}$) under FCFC BCs, where the natural modes computed by DSM are shown in the top whereas the bottom ones are computed by the FE software ANSYS.

Table 2

The first 8 natural frequencies ω (Hz) of free vibration for an individual rectangular membrane ($2 \text{ m} \times 1 \text{ m}$) under 9 classical BCs.

BCs	1	2	3	4	5	6	7	8
CCCC	(1,1) 23.506	(2,1) 29.733	(3,1) 37.902	(1,2) 43.343	(4,1) 47.012	(2,2) 47.012	(3,2) 52.561	(5,1) 56.610
FCFC	(0,1) 21.024	(1,1) 23.506	(2,1) 29.733	(3,1) 37.902	(0,2) 42.049	(1,2) 43.343	(2,2) 47.012	(4,1) 47.012
FCCC	(1,1) 21.671	(2,1) 26.280	(3,1) 33.655	(4,1) 42.376	(1,2) 42.376	(2,2) 44.908	(3,2) 49.586	(5,1) 51.767
FFFF	(0,0) 0	(1,0) 10.512	(0,1) 21.024	(2,0) 21.024	(1,1) 23.506	(2,1) 29.733	(3,0) 31.537	(0,1) 37.902
CFCF	(1,0) 10.512	(2,0) 21.024	(1,1) 23.506	(2,1) 29.733	(3,0) 31.537	(3,1) 37.902	(4,0) 42.049	(1,2) 43.343
FFCF	(1,0) 5.2561	(2,0) 15.768	(1,1) 21.671	(3,0) 26.280	(2,1) 26.280	(3,1) 33.655	(4,0) 36.793	(4,1) 42.376
CCCF	(1,1) 14.866	(2,1) 23.506	(3,1) 33.242	(1,2) 33.242	(2,2) 37.902	(4,1) 43.343	(3,2) 44.599	(4,2) 52.561
FCFF	(0,1) 10.512	(1,1) 14.866	(2,1) 23.506	(0,2) 31.537	(1,2) 33.242	(3,1) 33.242	(2,2) 37.902	(4,1) 43.343
FCCF	(1,1) 11.753	(2,1) 18.951	(3,1) 28.305	(1,2) 31.972	(2,2) 35.259	(4,1) 38.265	(3,2) 41.051	(5,1) 48.459

are computed in Table 4. It can be seen from Table 4 that, when the tension in one direction remains constant while that in the other direction increases, the natural frequency ω_{nm} will increase. As for the mode shapes, the half sine wave number in the direction with smaller tensile force will increase first. For example, when $T_y/T_x = 10$, the half sine wave number in the x direction increases first while that in the y direction remains unchanged.

Take CCCC BCs as an example, the natural frequency of a rectangular membrane is essentially the function of aspect ratio, tension ratio, half wave numbers in the x direction and y direction, namely, $\omega(\eta, \beta, m, n)$ (see Eq. (28)). If i) $\beta = T_y/T_x = 1, b \gg l$ or ii) $\eta = l/b = 0.5, T_y \gg T_x$, then the natural frequency is negligibly influenced by changes in the n value and is most influenced by variations in the m value, therefore, low frequency vibration is more likely to occur in the direction of longer edge or in the direction with smaller tension. It also can be explained from the physical sense, longer length and smaller tension represent higher flexibility and therefore result in more low frequency vibration modes. Hence, the vibration characteristics of a rectangular membrane can be improved by adjusting the aspect ratio η and tension ratio β according to $\omega_{nm}(\eta, \beta)$.

Table 3

The first 8 natural frequencies ω (Hz) of an individual equally stretched rectangular membrane with different aspect ratio η ($\eta=l/b=0.1, 0.5, 1, 2, 4, b=1$ m) under three typical BCs.

BCs	l/b	1	2	3	4	5	6	7	8
CCCC	0.1	(1,1) 211.29	(2,1) 214.41	(3,1) 219.50	(4,1) 226.44	(5,1) 235.06	(6,1) 245.18	(7,1) 256.64	(8,1) 269.24
	0.5	(1,1) 47.012	(2,1) 59.466	(3,1) 75.804	(1,2) 86.686	(4,1) 94.024	(2,2) 94.024	(3,2) 105.12	(5,1) 113.22
	1	(1,1) 29.733	(2,1) 47.012	(1,2) 47.012	(2,2) 59.466	(3,1) 66.485	(1,3) 66.485	(3,2) 75.804	(2,3) 75.804
	2	(1,1) 23.506	(1,2) 29.733	(1,3) 37.902	(2,1) 43.343	(2,2) 47.012	(1,4) 47.012	(2,3) 52.561	(1,5) 56.610
	4	(1,1) 21.671	(1,2) 23.506	(1,3) 26.280	(1,4) 29.733	(1,5) 33.655	(1,6) 37.902	(2,1) 42.376	(1,7) 42.376
FFFF	0.1	(0,0) 0	(1,0) 21.024	(2,0) 42.049	(3,0) 63.073	(4,0) 84.098	(5,0) 105.12	(6,0) 126.15	(7,0) 147.17
	0.5	(0,0) 0	(1,0) 21.024	(0,1) 42.049	(2,0) 42.049	(1,1) 47.012	(2,1) 59.466	(3,0) 63.073	(3,1) 75.804
	1	(0,0) 0	(0,1) 21.024	(1,0) 21.024	(1,1) 29.733	(0,2) 42.049	(2,0) 42.049	(1,2) 47.012	(2,1) 47.012
	2	(0,0) 0	(0,1) 10.512	(0,2) 21.024	(1,0) 21.024	(1,1) 23.506	(1,2) 29.733	(0,3) 31.537	(1,3) 37.902
	4	(0,0) 0	(0,1) 5.2561	(0,2) 10.512	(0,3) 15.768	(0,4) 21.024	(1,0) 21.024	(1,1) 21.671	(1,2) 23.506
FCFC	0.1	(0,1) 210.24	(1,1) 211.29	(2,1) 214.41	(3,1) 219.50	(4,1) 226.44	(5,1) 235.06	(6,1) 245.18	(7,1) 256.64
	0.5	(0,1) 42.049	(1,1) 47.012	(2,1) 59.466	(3,1) 75.804	(0,2) 84.098	(1,2) 86.686	(2,2) 94.024	(4,1) 94.024
	1	(0,1) 21.024	(1,1) 29.733	(0,2) 42.049	(1,2) 47.012	(2,1) 47.012	(2,2) 59.466	(0,3) 63.073	(1,3) 66.485
	2	(0,1) 10.512	(0,2) 21.024	(1,1) 23.506	(1,2) 29.733	(0,3) 31.537	(1,3) 37.902	(0,4) 42.049	(2,1) 43.343
	4	(0,1) 5.2561	(0,2) 10.512	(0,3) 15.768	(0,4) 21.024	(1,1) 21.671	(1,2) 23.506	(0,5) 26.280	(1,3) 26.280

Table 4

The first 8 natural frequencies ω (Hz) of an individual unequally stretched rectangular membrane with different tension ratio β ($\beta=T_y/T_x=0.1, 0.5, 2, 10, T_x=13800$ N/m, $l=1$ m, $b=2$ m) under three typical BCs.

Mode	1	2	3	4	5	6	7	8
CCCC								
$T_y/T_x = 0.1$	(1,1) 12.438	(1,2) 16.950	(2,1) 22.051	(1,3) 22.546	(2,2) 24.876	(1,4) 28.596	(2,3) 28.980	(3,1) 32.230
$T_y/T_x = 0.5$	(1,1) 18.208	(2,1) 25.749	(1,2) 31.537	(3,1) 34.865	(2,2) 36.415	(3,2) 43.343	(4,1) 44.599	(1,3) 45.822
$T_y/T_x = 2$	(1,1) 31.537	(2,1) 36.415	(3,1) 43.343	(4,1) 51.499	(5,1) 60.388	(1,2) 60.388	(2,2) 63.073	(3,2) 67.311
$T_y/T_x = 10$	(1,1) 67.311	(2,1) 69.730	(3,1) 73.585	(4,1) 78.666	(5,1) 84.752	(6,1) 91.643	(7,1) 99.172	(8,1) 107.20
FFFF								
$T_y/T_x = 0.1$	(0,0) 0	(0,1) 6.6485	(1,0) 10.512	(1,1) 12.438	(0,2) 13.297	(1,2) 16.950	(0,3) 19.945	(2,0) 21.024
$T_y/T_x = 0.5$	(0,0) 0	(1,0) 10.512	(0,1) 14.866	(1,1) 18.208	(2,0) 21.024	(2,1) 25.750	(0,2) 29.733	(3,0) 31.537
$T_y/T_x = 2$	(0,0) 0	(1,0) 10.512	(2,0) 21.024	(0,1) 29.733	(3,0) 31.537	(1,1) 31.537	(2,1) 36.415	(4,0) 42.049
$T_y/T_x = 10$	(0,0) 0	(1,0) 10.512	(2,0) 21.024	(3,0) 31.537	(4,0) 42.049	(5,0) 52.561	(6,0) 63.073	(0,1) 66.485
FCFC								
$T_y/T_x = 0.1$	(0,1) 6.6485	(1,1) 12.438	(0,2) 13.297	(1,2) 16.950	(0,3) 19.945	(2,1) 22.051	(1,3) 22.546	(2,2) 24.876
$T_y/T_x = 0.5$	(0,1) 14.866	(1,1) 18.208	(2,1) 25.750	(0,2) 29.733	(1,2) 31.537	(3,1) 34.865	(2,2) 36.415	(3,2) 43.343
$T_y/T_x = 2$	(0,1) 29.733	(1,1) 31.537	(2,1) 36.415	(3,1) 43.343	(4,1) 51.499	(0,2) 59.466	(5,1) 60.388	(1,2) 60.388
$T_y/T_x = 10$	(0,1) 66.485	(1,1) 67.311	(2,1) 69.730	(3,1) 73.585	(4,1) 78.666	(5,1) 84.752	(6,1) 91.643	(7,1) 99.172

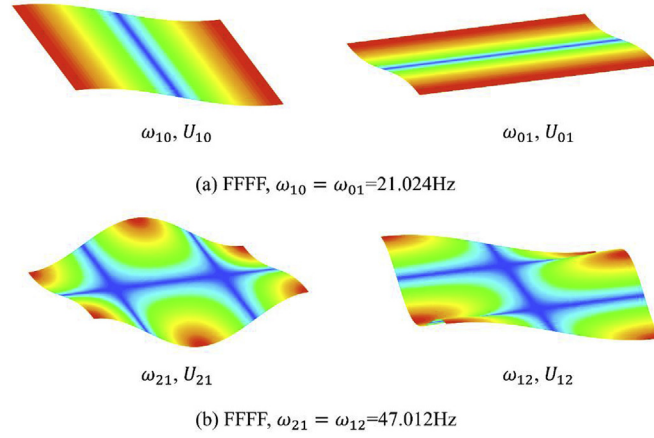


Fig. 7. Mode shapes of an individual equally stretched square membrane ($l = b = 1$ m) corresponding to repeated frequencies $\omega_{10}(=\omega_{01})$ and $\omega_{21}(=\omega_{12})$ under FFFF BCs.

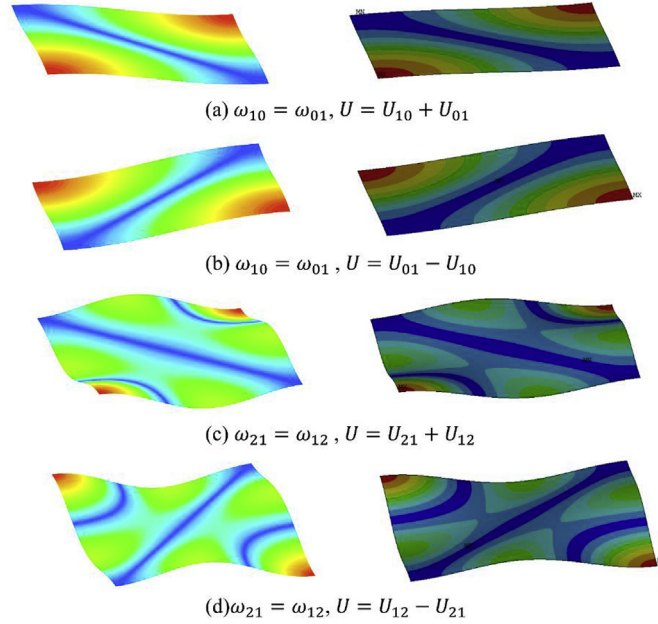


Fig. 8. Mode shapes for specific combinations of distinct natural modes U_{10} and U_{01} , U_{21} and U_{12} .

3.1.3. Some characteristics of free vibration mode shapes of individual rectangular membranes

From Sections 3.1.1 and 3.1.2, it can be found that the natural frequencies $\omega_{n_1 m_1}$ and $\omega_{n_2 m_2}$ can sometimes be equal. Without loss of generality, according to $\omega_{n_1 m_1} = \omega_{n_2 m_2}$, if the aspect ratio η and tension ratio β are rational numbers, the values of nonnegative integers m_1 , n_1 , m_2 and n_2 will satisfy the following equations

$$\left\{ \begin{array}{ll} \eta_1^2 n_1^2 + \beta_1 m_1^2 = \eta_2^2 n_2^2 + \beta_2 m_2^2, & \text{CCCC, FCFC, FFFF, CFCC} \\ \eta_1^2 \left(n_1 - \frac{1}{2}\right)^2 + \beta_1 m_1^2 = \eta_2^2 \left(n_2 - \frac{1}{2}\right)^2 + \beta_2 m_2^2 & \text{FCCC, FCCF} \\ \eta_1^2 n_1^2 + \beta_1 \left(m_1 - \frac{1}{2}\right)^2 = \eta_2^2 n_2^2 + \beta_2 \left(m_2 - \frac{1}{2}\right)^2, & \text{CCCF, FCFF} \\ \eta_1^2 \left(n_1 - \frac{1}{2}\right)^2 + \beta_1 \left(m_1 - \frac{1}{2}\right)^2 = \eta_2^2 \left(n_2 - \frac{1}{2}\right)^2 + \beta_2 \left(m_2 - \frac{1}{2}\right)^2, & \text{FCCF} \end{array} \right. \quad (36)$$

Take the case of CCCC boundary conditions (BCs) as an example, according to Eq. (28) (other BCs have similar expressions), $\omega_{n_1 m_1} = \pi c \sqrt{\left(\frac{n_1}{b}\right)^2 + \beta_1 \left(\frac{m_1}{l}\right)^2}$ and $\omega_{n_2 m_2} = \pi c \sqrt{\left(\frac{n_2}{b}\right)^2 + \beta_2 \left(\frac{m_2}{l}\right)^2}$, then $\eta_1^2 n_1^2 + \beta_1 m_1^2 = \eta_2^2 n_2^2 + \beta_2 m_2^2$ can be derived from $\omega_{n_1 m_1} = \omega_{n_2 m_2}$ as shown in Eq. (36). This means that the same frequency $\omega_{n_1 m_1} (= \omega_{n_2 m_2})$ corresponds to two different eigenfunctions $U_{n_1 m_1}(x, y)$ and $U_{n_2 m_2}(x, y)$. Next, this modal feature of rectangular membranes will be discussed in detail below.

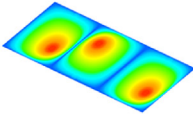
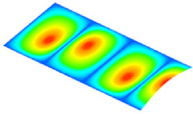
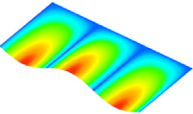
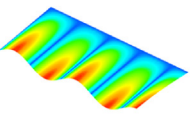
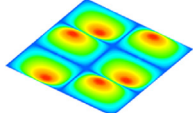
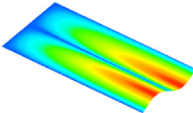
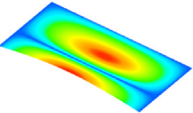
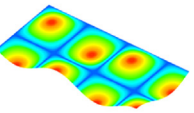
(1) Repeated eigenvalues with distinguishing mode shapes for equally stretched square membranes

When aspect ratio $\eta = 1$, tension ratio $\beta = 1$, based on Eq. (36), the relationship $\omega_{nm} = \omega_{mn}$ can be obtained under CCCC, FCFC, FFFF, CFCC, FCCF BCs. Fig. 7 displays the mode shapes of an individual equally stretched square membrane ($l = b = 1$ m) corresponding to repeated frequencies $\omega_{10} (= \omega_{01})$ and $\omega_{21} (= \omega_{12})$ under FFFF BCs. It can be seen that the corresponding natural modes U_{10} and U_{01} , U_{21} and U_{12} are different. When the mode shapes are computed by the FE software ANSYS, the results, however, are linear combinations of natural modes U_{10} and U_{01} , U_{21} and U_{12} . It is not difficult to see from Fig. 8 that the mode shapes computed by ANSYS corresponding to repeated frequencies $\omega_{10} (= \omega_{01})$ and $\omega_{21} (= \omega_{12})$ can be represented as $U_{01} \pm U_{10}$ and $U_{12} \pm U_{21}$. Therefore, if there are repeated natural frequencies ω_{nm} and ω_{mn} , any linear combination ($U = AU_{nm} + BU_{mn}$) of the corresponding distinct natural modes U_{nm} and U_{mn} can also be a natural mode of the membrane, which can be taken advantage of to transfer the energy from one mode to another.

(2) Repeated eigenvalues with distinguishing mode shapes for equally stretched rectangular membranes

Table 5

Mode shapes of individual equally stretched rectangular membranes (aspect ratio $\eta = l/b$) corresponding to repeated frequencies under four representative BCs.

CCCC	FCCC	CCCF	FCCF
$\omega_{31} = \omega_{23} = 75.804\text{Hz}$	$\omega_{41} = \omega_{12} = 42.376\text{Hz}$	$\omega_{31} = \omega_{12} = 33.242\text{Hz}$	$\omega_{51} = \omega_{42} = 48.459\text{Hz}$
			
$\eta_1 = 0.5, b = 1\text{m}$ 3 rd mode, ω_{31}	$\eta_1 = 0.5, b = 2\text{m}$ 4 th mode, ω_{41}	$\eta_1 = 0.5, b = 2\text{m}$ 3 rd mode, ω_{31}	$\eta_1 = 0.5, b = 2\text{m}$ 8 th mode, ω_{51}
			
$\eta_2 = 1, b = 1\text{m}$ 8 th mode, ω_{23}	$\eta_2 = 0.5, b = 2\text{m}$ 5 th mode, ω_{12}	$\eta_2 = 0.5, b = 2\text{m}$ 4 th mode, ω_{12}	$\eta_2 = 0.5, b = 2\text{m}$ 9 th mode, ω_{42}

In order to demonstrate two distinct natural modes $U_{n_1 m_1}$ and $U_{n_2 m_2}$ correspond to the same frequency $\omega_{n_1 m_1} (= \omega_{n_2 m_2})$ in equally stretched rectangular membranes, Table 5 exhibits the mode shapes of individual equally stretched rectangular membranes corresponding to repeated frequencies under CCCC, FCCC, CCCF and FCCF BCs. For instance, it can be seen from Table 5, the 3rd natural frequency ω_{31} where $\eta_1 = l/b = 0.5$ is equal to the 8th natural frequency ω_{23} where $\eta_2 = l/b = 1$ under CCCC BCs, but the corresponding natural modes are different.

(3) Repeated eigenvalues with distinguishing mode shapes for unequally stretched rectangular membranes

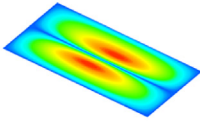
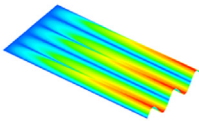
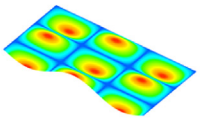
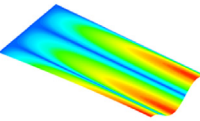
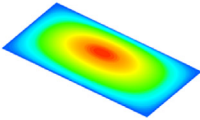
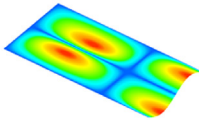
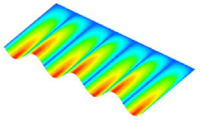
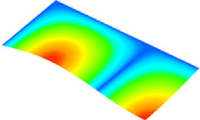
In order to demonstrate two distinct natural modes $U_{n_1 m_1}$ and $U_{n_2 m_2}$ correspond to the same frequency $\omega_{n_1 m_1} (= \omega_{n_2 m_2})$ in unequally stretched rectangular membranes, Table 6 presents the mode shapes of individual unequally stretched rectangular membranes ($l = 1$ m, $b = 2$ m, $\beta = T_y/T_x = 0.1, 0.5, 2, 10$, $T_x = 13800$ N/m) corresponding to repeated frequencies under CCCC, FCCC, CCCF and FCCF BCs. According to Table 6, for example, the 3rd natural frequency ω_{12} where $\beta_1 = T_y/T_x = 0.5$ is equal to the 1st natural frequency ω_{11} where $\beta_2 = T_y/T_x = 2$ under CCCC BCs, but the corresponding natural modes are different.

3.2. Membrane assembly

Consider a membrane assembly composed of seven membrane elements as shown in Fig. 9 (b_1 and T_{y1} are the length and tension per unit length in the y direction of membrane elements E1, E3, E5 and E7 whereas b_2 and T_{y2} are those of membrane elements E2, E4 and E6, the magnitudes of ρ for each membrane element are equal to facilitate the comparison with the finite element method (FEM), L_1, L_2, L_3 and L_4 are the four sides of the membrane assembly and $L_1 = L_3 = l = 2$ m, $L_2 = L_4 = 4b_1 + 3b_2$, $b_1 = 2$ m, $b_2 = 1$ m, $T_x = T_{y2} = 13800$ N/m, $T_{y1} = 6900$ N/m, $\rho = 7.805$ kg/m²). There are also nine classical boundary conditions for a membrane assembly and Table 7 shows the first 8 natural frequencies of free vibration for the membrane

Table 6

Mode shapes of individual unequally stretched rectangular membranes ($\eta_1 = \eta_2 = l/b = 0.5$, $b = 2$ m, $\beta = T_y/T_x$, $\beta_1 \neq \beta_2$) corresponding to repeated frequencies under four representative BCs.

CCCC	FCCC	CCCF	FCCF
$\omega_{12} = \omega_{11} = 31.537\text{Hz}$	$\omega_{15} = \omega_{22} = 33.655\text{Hz}$	$\omega_{33} = \omega_{71} = 80.746\text{Hz}$	$\omega_{13} = \omega_{21} = 17.432\text{Hz}$
			
$\beta_1 = 0.5, 3^{\text{rd}} \text{ mode}, \omega_{12}$	$\beta_1 = 0.1, 12^{\text{th}} \text{ mode}, \omega_{15}$	$\beta_1 = 2, 16^{\text{th}} \text{ mode}, \omega_{33}$	$\beta_1 = 0.1, 4^{\text{th}} \text{ mode}, \omega_{13}$
			
$\beta_2 = 2, 1^{\text{st}} \text{ mode}, \omega_{11}$	$\beta_2 = 2, 5^{\text{th}} \text{ mode}, \omega_{22}$	$\beta_2 = 10, 7^{\text{th}} \text{ mode}, \omega_{71}$	$\beta_2 = 0.5, 2^{\text{nd}} \text{ mode}, \omega_{21}$

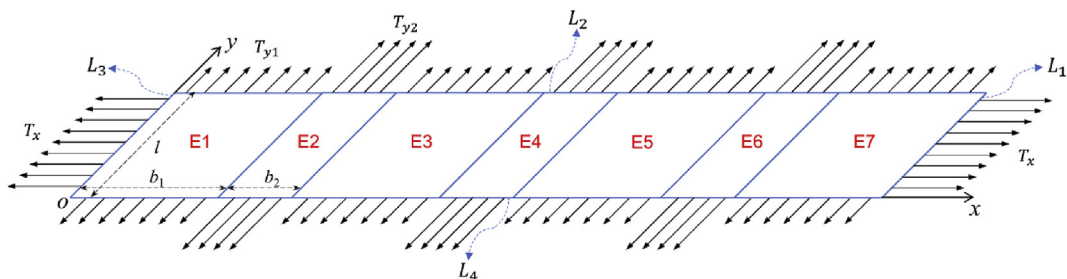


Fig. 9. Membrane assembly.

Table 7

The first 8 natural frequencies ω (Hz) of free vibration for a membrane assembly ($\rho = 7.805 \text{ kg/m}^2$, $T_x = T_{y2} = 13800 \text{ N/m}$, $T_{y1} = 6900 \text{ N/m}$, $l = 2 \text{ m}$, $b_1 = 2 \text{ m}$, $b_2 = 1 \text{ m}$) under all nine BCs by using the DSM and FEM.

BCs	Method	1	2	3	4	5	6	7	8
CCCC	DSM	17.318	18.554	20.651	21.722	25.577	28.567	32.039	32.713
	FEM	17.544	18.728	20.630	22.238	25.455	28.414	31.452	34.193
FCFC	DSM	16.227	16.340	17.861	19.526	23.702	25.596	28.344	30.928
	FEM	16.369	16.535	18.146	19.968	23.183	25.444	28.343	31.178
FCCC	DSM	16.278	17.538	19.032	21.204	24.356	26.978	29.974	30.928
	FEM	16.385	17.765	19.289	21.439	24.090	26.875	29.904	31.189
FFFF	DSM	0	3.8226	7.6452	11.468	15.290	16.227	16.340	17.861
	FEM	0	3.8225	7.6448	11.466	15.275	16.352	16.503	18.103
CFCF	DSM	3.8226	7.6452	11.468	15.290	17.318	18.554	19.113	20.652
	FEM	3.8225	7.6446	11.466	15.286	17.483	18.672	19.102	20.606
FFCF	DSM	1.9113	5.7339	9.5565	13.379	16.265	16.984	17.202	18.779
	FEM	1.9113	5.7337	9.5558	13.376	16.359	17.716	17.195	19.228
CCCF	DSM	9.3708	11.502	14.449	17.128	20.864	24.446	25.156	25.915
	FEM	9.3979	11.488	14.344	17.274	20.830	24.345	25.736	26.612
FCFF	DSM	8.3173	8.9612	11.133	13.924	17.758	20.906	23.649	23.660
	FEM	8.3484	8.9901	11.185	14.033	17.551	20.830	23.858	24.085
FCCF	DSM	8.5238	10.130	12.683	15.776	19.166	22.642	23.654	25.224
	FEM	8.5394	10.145	12.694	15.774	19.103	22.574	23.871	25.705

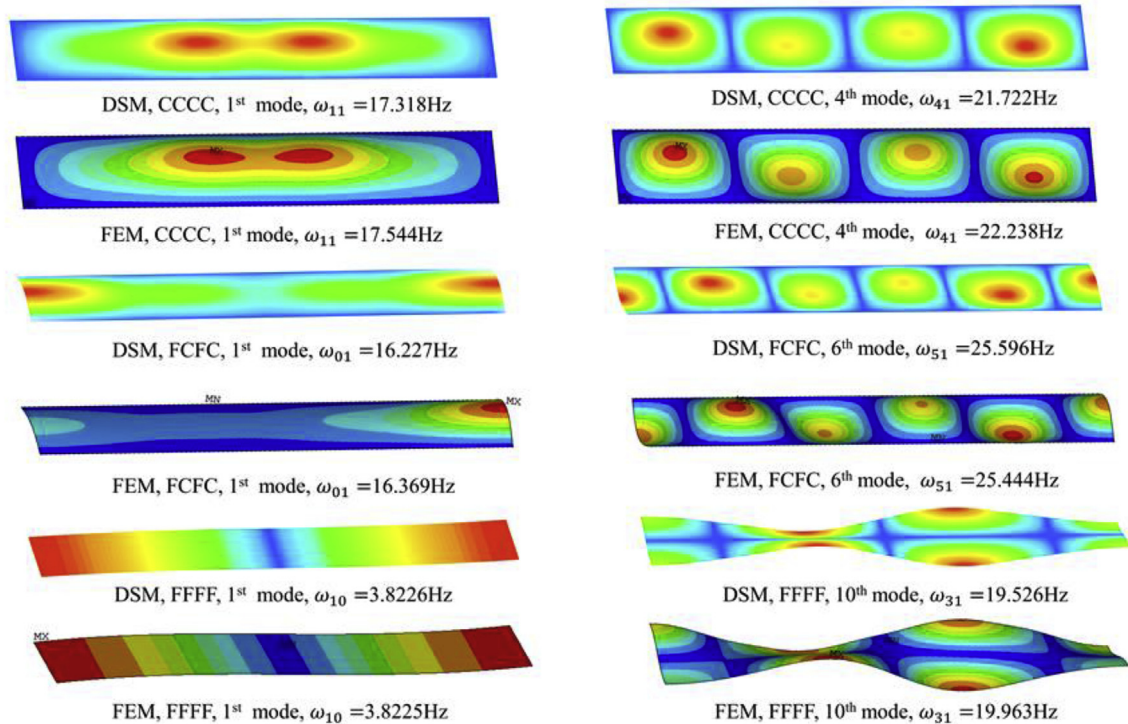


Fig. 10. Some mode shapes of the membrane assembly under three typical BCs by using the DSM and FEM.

assembly under all nine BCs (the BCs are listed in the anticlockwise sense of $L_1 - L_2 - L_3 - L_4$) computed by the DSM and FEM (mesh size is 550×100). It takes 76 s for the FEM to compute the first 200 modes of the membrane assembly while the DSM only takes 0.25 s but gives exact results, therefore, the DSM still has higher computational efficiency in a membrane assembly. Some representative mode shapes are shown in Fig. 10.

It can be seen from Table 7 and Fig. 10 that the results computed by the DSM and FEM agree very well. It is obvious that the DSM can be applied to the membrane assemblies in a quite general sense, such as the assembly of membrane elements with different density, tension and length, which covers a very wide application scope in engineering problems.

4. Conclusions

A dynamic stiffness (DS) matrix has been developed for free vibration of rectangular membranes subjected to any arbitrary boundary conditions. The dynamic stiffness formulation for membrane elements is based on the exact general solutions of the governing differential equation under three different principal boundary conditions (PBCs). The force and displacement boundary conditions on the nodal boundaries (NB) are correlated in the form the dynamic stiffness matrices by eliminating unknown coefficients from the general solutions. The explicit expressions of DS matrices for membrane elements under all three kinds of PBCs are obtained. Then, the membrane elements are assembled to form the global DS matrix of the final complex structure and any nodal boundary conditions can be applied. Then, the well-known Wittrick-Williams (WW) algorithm is applied to compute the natural frequencies. The analytical expressions of J_0 count in the WW algorithm under all PBCs are derived.

An accurate and computationally efficient program has been developed using the DSM for membranes and their assemblies. Several numerical examples have been conducted to compute the natural frequencies and representative mode shapes for all possible combinations of boundary conditions. Results are validated against those obtained by the conventional FEM. It can be concluded that the proposed DSM can give exact results for both individual membranes and complex assemblies by using very few number of membrane elements. Thus, the proposed method has the advantage over the conventional FEM in high computational efficiency, exactness and robustness. In addition, note that the obtained mode shapes corresponding to the repeated natural frequency are completely different, which are related to certain aspect ratio and tension ratio. The DSM presented in this study can be extended to more 2D domains with other geometry such as circular, annular, sectorial, elliptical and complex shaped membrane structures and with arbitrary classical [52,58,61,62] and nonclassical [63,64] boundary conditions. Furthermore, this method sheds lights on future studies on acoustic cavity, heat transfer, as well as harbor resonance problems.

Declaration of competing interest

The authors declare that they have no known competing financial interests or personal relationships that could have appeared to influence the work reported in this paper.

CRediT authorship contribution statement

Xiang Liu: Conceptualization, Methodology, Writing - review & editing, Supervision, Project administration, Funding acquisition. **Xueyi Zhao:** Investigation, Data curation, Writing - original draft, Writing - review & editing. **Chen Xie:** Writing - review & editing.

Acknowledgements

The authors appreciate the supports from the National Key R&D Program of China (Grant No. 2018YFB1201603-03), National Natural Science Foundation (Grant No. 11802345), State Key Laboratory of High Performance Complex Manufacturing (Grant No. ZZYJKT2019-07) and Initial Funding of Specially-appointed Professorship (Grant No. 502045001) which made this research possible.

References

- [1] J.L. Gaspar, M.J. Solter, S. Pappa R, Membrane scanning vibration laser studies using a laser vibrometer, in: 20th International Modal Analysis Conference, 2002.
- [2] S. Kukathanan, S. Pellegrino, Vibration of Prestressed Membrane Reflectors, University of Cambridge, Department of Engineering Cambridge, UK, 2001.
- [3] J. Rehder, P. Rombach, O. Hansen, Magnetic flux generator for balanced membrane loudspeaker, *Sens. Actuators, A Phys.* 97–98 (2002) 61–67.
- [4] M.A. Shah, I.A. Shah, D.-G. Lee, S. Hur, Design approaches of MEMS microphones for enhanced performance, *J. Sensors* 2019 (4) (2019) 1–26.
- [5] S.M. Hasheminejad, S. Rezaei, P. Hosseini, Exact solution for dynamic response of an elastic elliptical membrane, *Thin-Walled Struct.* 49 (2) (2011) 371–378.
- [6] H.P.W. Gottlieb, Exact vibration solutions for some irregularly shaped membranes and simply supported plates, *J. Sound Vib.* 103 (3) (1985) 333–339.
- [7] A.W. Leissa, Closed form exact solutions for the steady state vibrations of continuous systems subjected to distributed exciting forces, *J. Sound Vib.* 134 (3) (1989) 435–453.
- [8] J.-H. Kang, Closed form exact solutions of viscously damped free and forced vibrations of rectangular membranes, *J. Vib. Contr.* 24 (10) (2018) 2096–2106.
- [9] K. Sato, Forced vibration analysis of a composite rectangular membrane consisting of strips, *J. Sound Vib.* 63 (3) (1979) 411–417.
- [10] P. Amore, Solving the Helmholtz equation for membranes of arbitrary shape: numerical results, *J. Phys. A Math. Theor.* 41 (26) (2008) 265206.
- [11] P. Amore, A new method for studying the vibration of non-homogeneous membranes, *J. Sound Vib.* 321 (1–2) (2009) 104–114.
- [12] P. Amore, F.M. Fernandez, M. Rodriguez, Accurate calculation of the eigenvalues of non-uniform strings and membranes, *Open Phys.* 10 (4) (2012) 913–925.
- [13] S. Durvasula, Natural frequencies and modes of skew membranes, *J. Acoust. Soc. Am.* 44 (6) (1968) 1636–1646.
- [14] D.J. Gorman, R.K. Singhal, A superposition-Rayleigh-Ritz method for free vibration analysis of non-uniformly tensioned membranes, *J. Sound Vib.* 162 (3) (1993) 489–501.
- [15] L. Bauer, E.L. Reiss, Free vibrations of rhombic plates and membranes, *J. Acoust. Soc. Am.* 54 (5) (1973) 1373–1375.
- [16] J.T. Chen, S.K. Kao, W.M. Lee, Y.T. Lee, Eigensolutions of the Helmholtz equation for a multiply connected domain with circular boundaries using the multipole Trefftz method, *Eng. Anal. Bound. Elem.*, Elsevier 34 (5) (2010) 463–470.

- [17] J.R. Chang, R.F. Liu, W. Yeih, S.R. Kuo, Applications of the direct Trefftz boundary element method to the free-vibration problem of a membrane, *J. Acoust. Soc. Am.* 112 (2) (2002) 518–527.
- [18] J.R. Chang, R.F. Liu, An asymmetric indirect Trefftz method for solving free-vibration problems, *J. Sound Vib.* 275 (3–5) (2004) 991–1008.
- [19] H. Ersoy, Civallek Ö, L. Özpolatb, Free vibration analysis of rectangular membranes with variable density using the discrete singular convolution approach, *Asian J. Civ. Eng.* 11 (1) (2010) 83–94.
- [20] Ö. Civallek, Eigenvalues of membranes having skew and rhombic geometry using discrete singular convolution algorithm, *Commun. Nonlinear Sci. Numer. Simulat.* 14 (11) (2009) 4003–4009.
- [21] G.W. Wei, Vibration analysis by discrete singular convolution, *J. Sound Vib.* 244 (3) (2001) 535–553.
- [22] S.W. Kang, S.N. Atluri, Improved non-dimensional dynamic influence function method based on tow-domain method for vibration analysis of membranes, *Adv. Mech. Eng.* 7 (2) (2015) 1–8.
- [23] S.W. Kang, J.M. Lee, Application of free vibration analysis of membranes using the non-dimensional dynamic influence function, *J. Sound Vib.* 234 (3) (2000) 455–470.
- [24] S.W. Kang, J.M. Lee, Y.J. Kang, Vibration analysis of arbitrarily shaped membranes using non-dimensional dynamic influence function, *J. Sound Vib.* 221 (1) (1999) 117–132.
- [25] Ouakad, Free vibration characteristics of rectangular membranes assuming rounded-edges boundary, *Vibration* 2 (3) (2019) 265–270.
- [26] M. Nikkhah-Bahrami, M. Loghmani, M. Pooyanfar, A new analytical approach for free vibration of membrane from wave standpoint, *Int. J. Mech. Mechatron. Eng.* 2 (5) (2008) 662–665.
- [27] A. Bahrami, A. Teimourian, Study on vibration, wave reflection and transmission in composite rectangular membranes using wave propagation approach, *Meccanica* 52 (1–2) (2016) 231–249.
- [28] H.W. Lee, S.Y. Hong, D.H. Park, H.W. Kwon, Energy flow boundary element method for vibration analysis of one and two dimension structures, *Shock Vib.* 15 (1) (2008) 33–50.
- [29] J.T. Katsikadelis, E.J. Sapountzakis, An approach to the vibration problem of homogeneous, non-homogeneous and composite membranes based on the boundary element method, *Int. J. Numer. Methods Eng.* 26 (11) (1988) 2439–2455.
- [30] R. Heuer, H. Irshchik, A boundary element method for eigenvalue problems of polygonal membranes and plates, *Acta Mech.* 66 (1–4) (1987) 9–20.
- [31] S.H. Chen, W.J. Lin, A.Y.T. Leung, Finite element vibration analysis of rectangular membrane, *AIP Conf. Proc.* 1233 (1) (2010) 1612–1617. New York: American Institute of Physics.
- [32] W.H. Chen, C.W. Wu, Adaptable spline element for membrane vibration analysis, *Int. J. Numer. Methods Eng.* 39 (14) (1996) 2457–2476.
- [33] G.R. Buchanan, J. Peddieson, A finite element in elliptic coordinates with application to membrane vibration, *Thin-Walled Struct.* 43 (9) (2005) 1444–1454.
- [34] A. Houmat, Hierarchical finite element analysis of the vibration of membranes, *J. Sound Vib.* 201 (4) (1997) 465–472.
- [35] N. Fantuzzi, F. Tornabene, E. Viola, Generalized differential quadrature finite element method for vibration analysis of arbitrarily shaped membranes, *Int. J. Mech. Sci.* 79 (3) (2014) 216–251.
- [36] A. Houmat, A sector Fourier p-element for free vibration analysis of sectorial membranes, *Comput. Struct.* 79 (12) (2001) 1147–1152.
- [37] A.Y.T. Leung, B. Zhu, J. Zheng, H. Yang, A trapezoidal Fourier p-element for membrane vibrations, *Thin-Walled Struct.* 41 (5) (2003) 479–491.
- [38] N. Fantuzzi, G. Della Puppa, F. Tornabene, M. Trautz, Strong Formulation IsoGeometric Analysis for the vibration of thin membranes of general shape, *Int. J. Mech. Sci.* 120 (1) (2017) 322–340.
- [39] J. Park, I. Park, U. Lee, Transverse vibration and waves in a membrane: frequency domain spectral element modeling and analysis, *Math. Probl Eng.* 2014 (5) (2014) 1–14.
- [40] T. Kim, U. Lee, Exact spectral element model for rectangular membranes subjected to transverse vibrations, *Int. J. Mech. Sci.* 165 (2020) 105191.
- [41] J.T. Chen, J.W. Lee, L.L. Chen, P.S. Kuo, On the null and nonzero fields for true and spurious eigenvalues of annular and confocal elliptical membranes, *Eng. Anal. Bound. Elem., Elsevier* 37 (1) (2013) 42–59.
- [42] J.T. Chen, C.T. Chen, L.L. Chen, Null-field integral equation approach for eigenproblems with circular boundaries, *J. Comput. Acoust.* 15 (4) (2007) 401–428.
- [43] J.T. Chen, J.W. Lee, S.Y. Leu, Analytical and numerical investigation for true and spurious eigensolutions of an elliptical membrane using the real-part dual BIEM/BEM, *Meccanica* 47 (5) (2012) 1103–1117.
- [44] L.L. Chen, J.T. Chen, W.M. Lee, S.K. Kao, Computer assisted proof of spurious eigensolution for annular and eccentric membranes, *J. Mar. Sci. Technol.* 17 (3) (2009) 203–215.
- [45] W.H. Wittrick, F.W. Williams, A general algorithm for computing natural frequencies of elastic structures, *Q. J. Mech. Appl. Math.* 24 (3) (1971) 263–284.
- [46] J.R. Banerjee, S.A. Fisher, Coupled bending-torsional dynamic stiffness matrix for axially loaded beam elements, *Int. J. Numer. Methods Eng.* 33 (4) (1992) 739–751.
- [47] J.R. Banerjee, F.W. Williams, Coupled bending-torsional dynamic stiffness matrix of an axially loaded timoshenko beam element, *Int. J. Solid Struct.* 31 (6) (1994) 749–762.
- [48] J.R. Banerjee, Free vibration analysis of a twisted beam using the dynamic stiffness method, *Int. J. Solid Struct.* 38 (38–39) (2001) 6703–6722.
- [49] M.S. Anderson, F.W. Williams, Errata-BUNVIS-RG: exact frame buckling and vibration program, with repetitive geometry and substructuring, *J. Spacecraft Rockets* 25 (4) (1988), 96–96.
- [50] W.H. Wittrick, F.W. Williams, Buckling and vibration of anisotropic or isotropic plate assemblies under combined loadings, *Int. J. Mech. Sci.* 16 (4) (1974) 209–239.
- [51] J.R. Banerjee, S.O. Papkov, X. Liu, D. Kennedy, Dynamic stiffness matrix of a rectangular plate for the general case, *J. Sound Vib.* 342 (2015) 177–199.
- [52] X. Liu, J.R. Banerjee, Free vibration analysis for plates with arbitrary boundary conditions using a novel spectral-dynamic stiffness method, *Comput. Struct.* 164 (2016) 108–126.
- [53] J.B. Casimir, S. Kevorkian, T. Vinh, The dynamic stiffness matrix of two-dimensional elements: application to Kirchhoff's plate continuous elements, *J. Sound Vib.* 287 (3) (2005) 571–589.
- [54] N. Kolarevic, M. Nefovska-Danilovic, M. Petronijevic, Dynamic stiffness elements for free vibration analysis of rectangular Mindlin plate assemblies, *J. Sound Vib.* 359 (2015) 84–106.
- [55] X. Liu, C. Xie, H.C. Dan, Exact free vibration analysis for plate built-up structures under comprehensive combinations of boundary conditions, *Shock Vib.* (2020) 5305692, <https://doi.org/10.1155/2020/5305692>.
- [56] M. Boscolo, J.R. Banerjee, Dynamic stiffness formulation for composite Mindlin plates for exact modal analysis of structures. Part I: Theory, *Comput. Struct.* 96–97 (2012) 61–73.
- [57] E. Damnjanović, M. Marjanović, M. Nefovska-Danilović, Free vibration analysis of stiffened and cracked laminated composite plate assemblies using shear-deformable dynamic stiffness elements, *Compos. Struct.* 180 (2017) 723–740.
- [58] X. Liu, J.R. Banerjee, An exact spectral-dynamic stiffness method for free flexural vibration analysis of orthotropic composite plate assemblies - Part I: Theory, *Compos. Struct.* 132 (2015) 1274–1287.
- [59] X. Liu, X. Liu, S. Xie, A highly accurate analytical spectral flexibility formulation for buckling and wrinkling of orthotropic rectangular plates, *Int. J. Mech. Sci.* 168 (2020) 105311, <https://doi.org/10.1016/j.ijmecsci.2019.105311>.
- [60] X. Liu, X. Liu, W. Zhou, An analytical spectral stiffness method for buckling of rectangular plates on Winkler foundation subject to general boundary conditions, *Appl. Math. Model.* (2020), <https://doi.org/10.1016/j.apm.2020.05.010>.
- [61] X. Liu, J.R. Banerjee, A spectral dynamic stiffness method for free vibration analysis of plane elastodynamic problems, *Mech. Syst. Signal Process.* 87 (2017) 136–160.

- [62] X. Liu, J.R.R. Banerjee, An exact spectral-dynamic stiffness method for free flexural vibration analysis of orthotropic composite plate assemblies - Part II: Applications, *Compos. Struct.* 132 (2015) 1274–1287.
- [63] X. Liu, Spectral dynamic stiffness formulation for inplane modal analysis of composite plate assemblies and prismatic solids with arbitrary classical/nonclassical boundary conditions, *Compos. Struct.* 158 (2016) 262–280.
- [64] X. Liu, H.I. Kassem, J.R. Banerjee, An exact spectral dynamic stiffness theory for composite plate-like structures with arbitrary non-uniform elastic supports, mass attachments and coupling constraints, *Compos. Struct.* 142 (2016) 140–154.